Electronic Supplementary Information for

Syntheses and electronic, electrochemical, and theoretical studies of a series of μ-Oxo-triruthenium carboxylates bearing orthometalated phenazines

Camila F.N. da Silva,[1] Malik Al-Afyouni,[2] Congcong Xue,[2] Frederico Henrique do C. Ferreira,[3] Luiz Antônio S. Costa,[3] Claudia Turro,[2] Sofia Nikolaou[1]*

[1]LABIQSC[2] – Laboratório de Atividade Biológica e Química Supramolecular de Composto de Coordenação, Departamento de Química, Faculdade de Filosofia, Ciências e Letras de Ribeirão Preto, Universidade de São Paulo, Av. Bandeirantes 3900, 14040-901, Ribeirão Preto - SP, Brazil.

[2]Department of Chemistry and Biochemistry, The Ohio State University, Columbus, Ohio 43210, United States.

[3]NEQC - Núcleo de Estudos em Química Computacional, Departamento de Química, ICE, Universidade Federal de Juiz de Fora, Juiz de Fora 36036-900, Minas Gerais, Brazil.

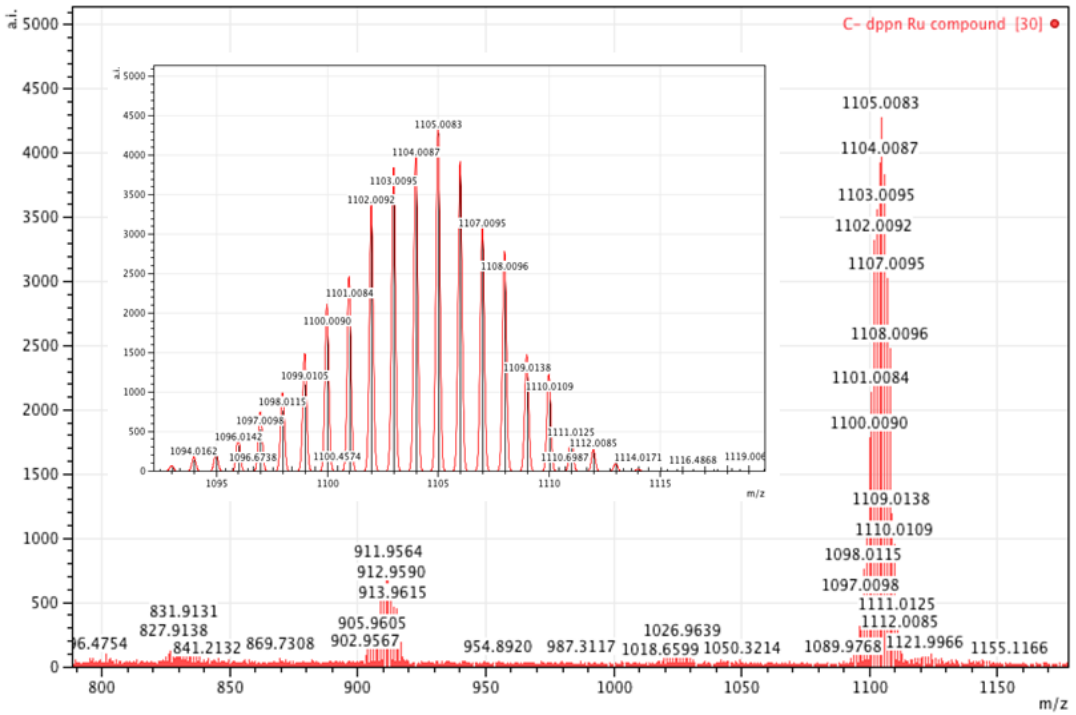

Figure ESI1. ESI-MS spectrum of $[Ru_3(\mu_3\text{-}O)(\mu\text{-}OAc)_5\{\mu\text{-}\eta^1(C),\eta^2(N,N)\text{-}dppn\}(py)_2]^+$ ion. The inset shows the molecular ion at m/z 1105 detected in ESI-MS spectrum, with emphasis on the isotopic pattern of the Ru_3 unit (the gray bar inside each peak corresponds to the theoretically predicted isotopic pattern).

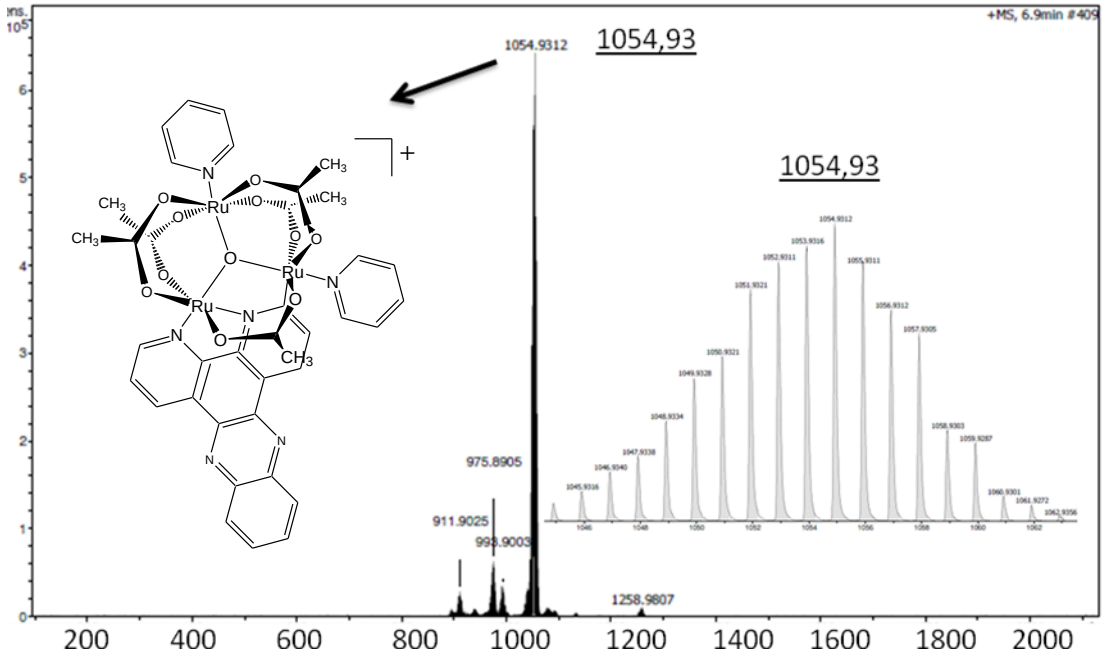

Figure ESI2. ESI-MS spectrum of $[Ru_3(\mu_3\text{-}O)(\mu\text{-}OAc)_5\{\mu\text{-}\eta^1(C),\eta^2(N,N)\text{-}dppz\}(py)_2]^+$ ion. The inset shows the molecular ion at m/z 1055 detected in ESI-MS spectrum, with emphasis on the isotopic pattern of the Ru_3 unit (the gray bar inside each peak corresponds to the theoretically predicted isotopic pattern).

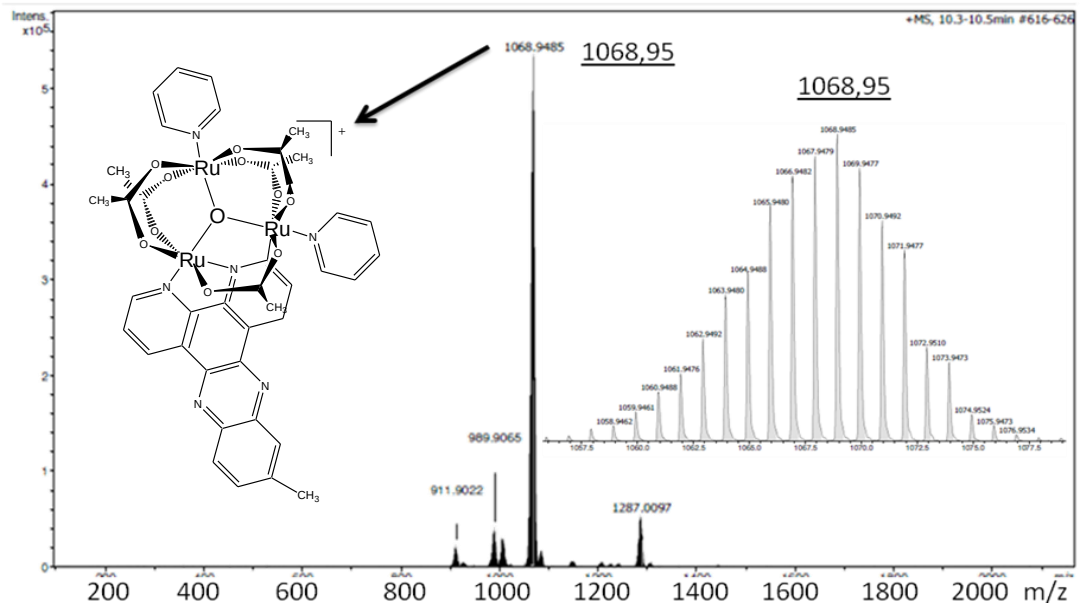

Figure ESI3. ESI-MS spectrum of $[Ru_3(\mu_3\text{-}O)(\mu\text{-}OAc)_5\{\mu\text{-}\eta^1(C),\eta^2(N,N)\text{-}dppzCH_3\}(py)_2]^+$ ion. The inset shows the molecular ion at m/z 1069 detected in ESI-MS spectrum, with emphasis on the isotopic pattern of the Ru_3 unit (the gray bar inside each peak corresponds to the theoretically predicted isotopic pattern).

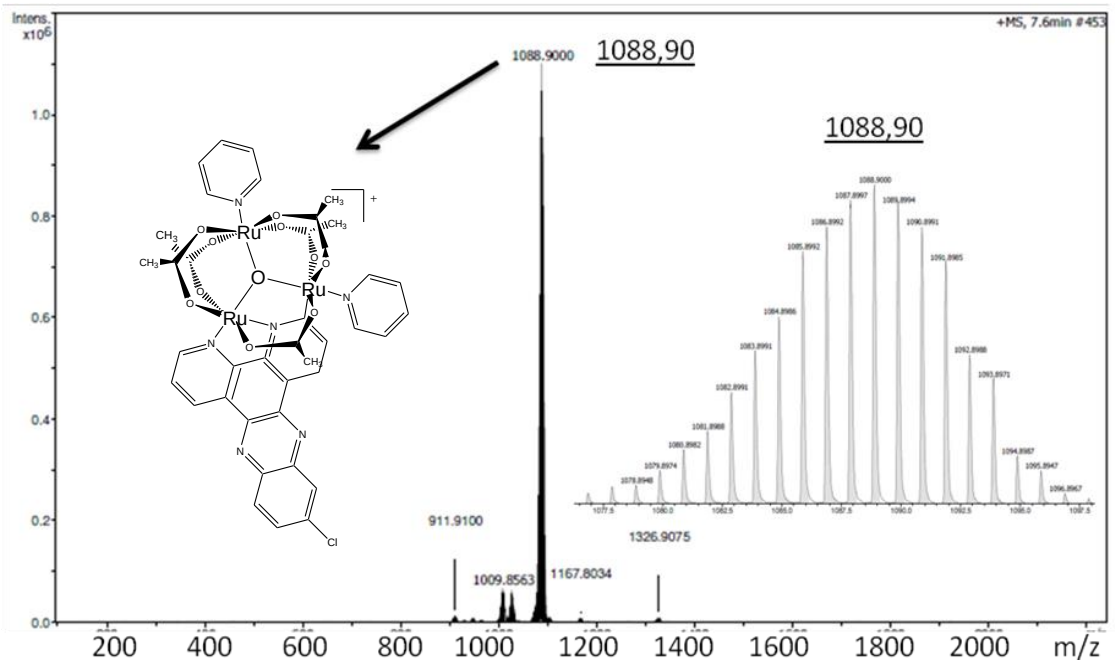

Figure ESI4. ESI-MS spectrum of $[Ru_3(\mu_3\text{-}O)(\mu\text{-}OAc)_5\{\mu\text{-}\eta^1(C),\eta^2(N,N)\text{-}dppzCl\}(py)_2]^+$ ion. The inset shows the molecular ion at m/z 1089 detected in ESI-MS spectrum, with emphasis on the isotopic pattern of the Ru_3 unit (the gray bar inside each peak corresponds to the theoretically predicted isotopic pattern).

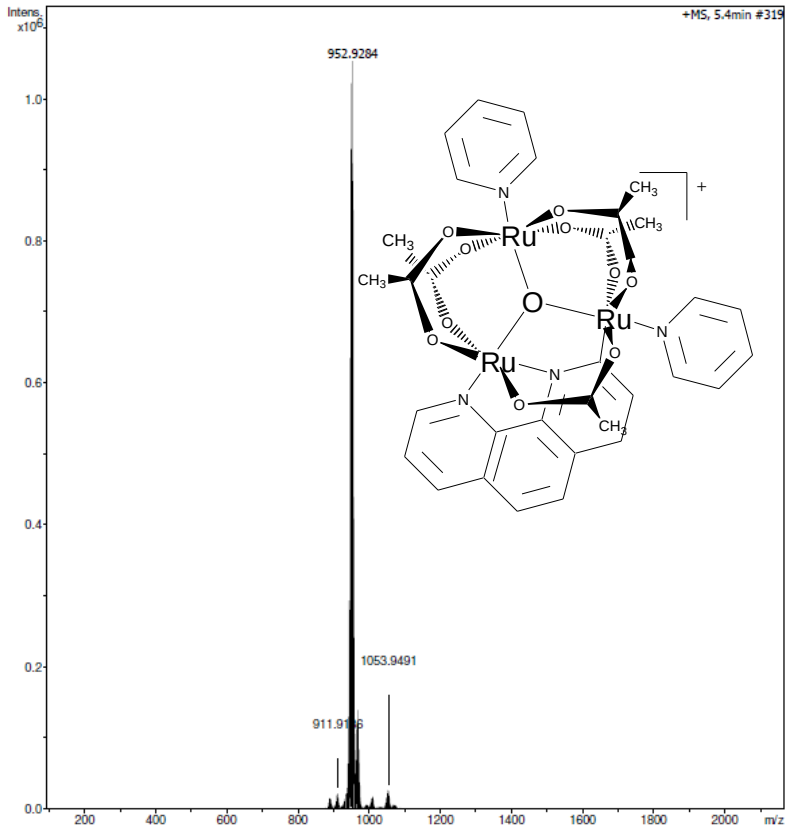

Figure ESI5. ESI-MS spectrum of $[Ru_3(\mu_3\text{-}O)(\mu\text{-}OAc)_5\{\mu\text{-}\eta^1(C),\eta^2(N,N)\text{-}phen\}(py)_2]^+$.

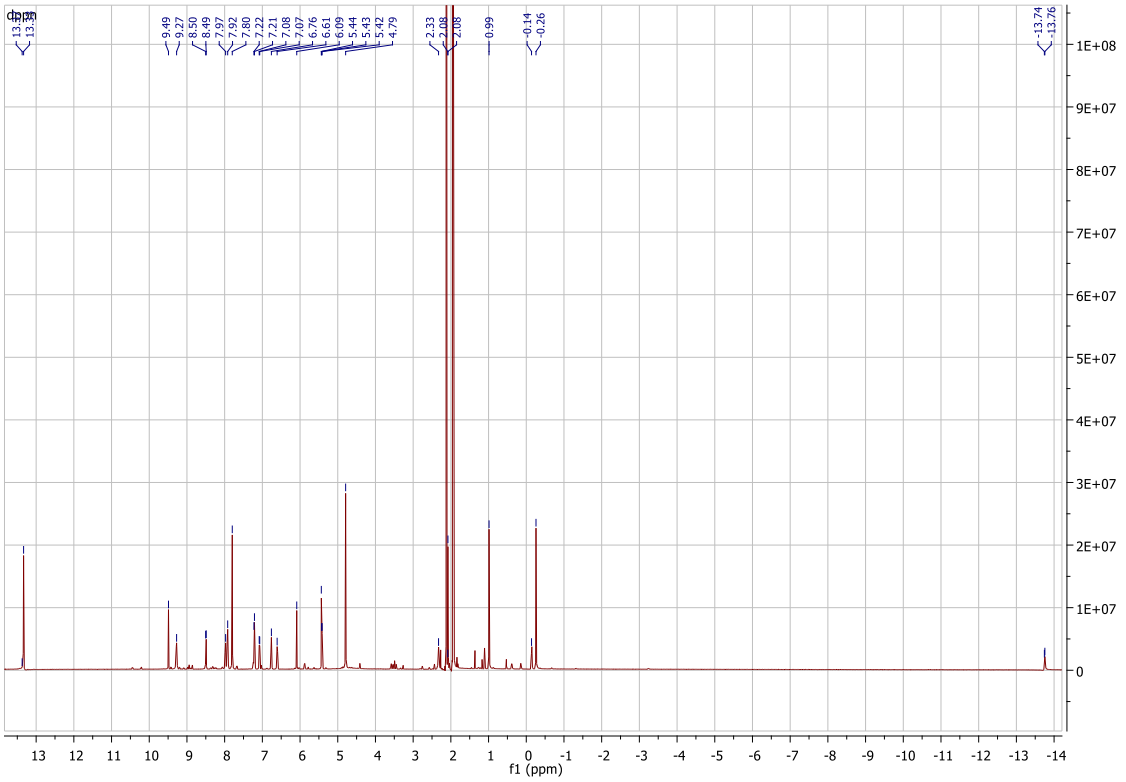

Figures ESI6. ^1H NMR spectrum of compound **1** $[Ru_3(\mu_3\text{-}O)(\mu\text{-}OAc)_5\{\mu\text{-}\eta^1(C),\eta^2(N,N)\text{-}dppn\}(py)_2]PF_6$, recorded from 10^{-2} mol L^{-1} acetonitrile-$_{d3}$ solution.

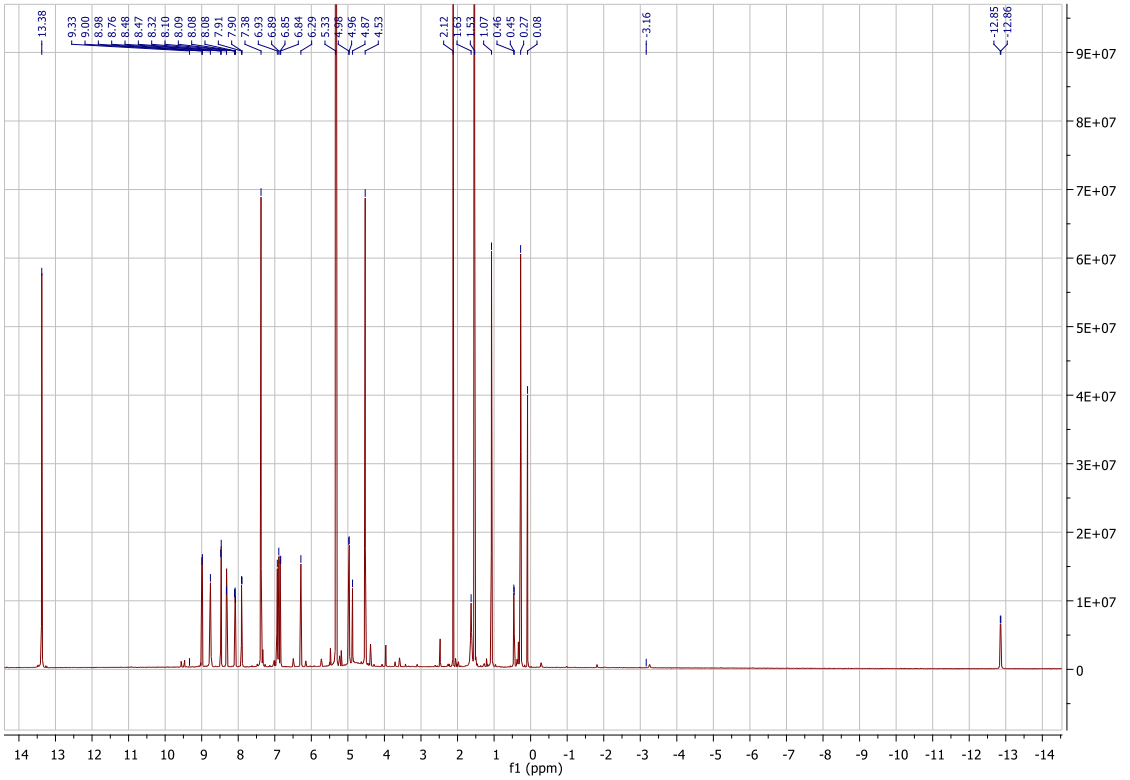

Figures ESI7. ^{1}H NMR spectrum of compound **2** $[Ru_3(\mu_3\text{-}O)(\mu\text{-}OAc)_5\{\mu\text{-}\eta^1(C),\eta^2(N,N)\text{-}dppz\}(py)_2]PF_6$, recorded from 10^{-2} mol L^{-1} dichloromethane-$_{d2}$ solution.

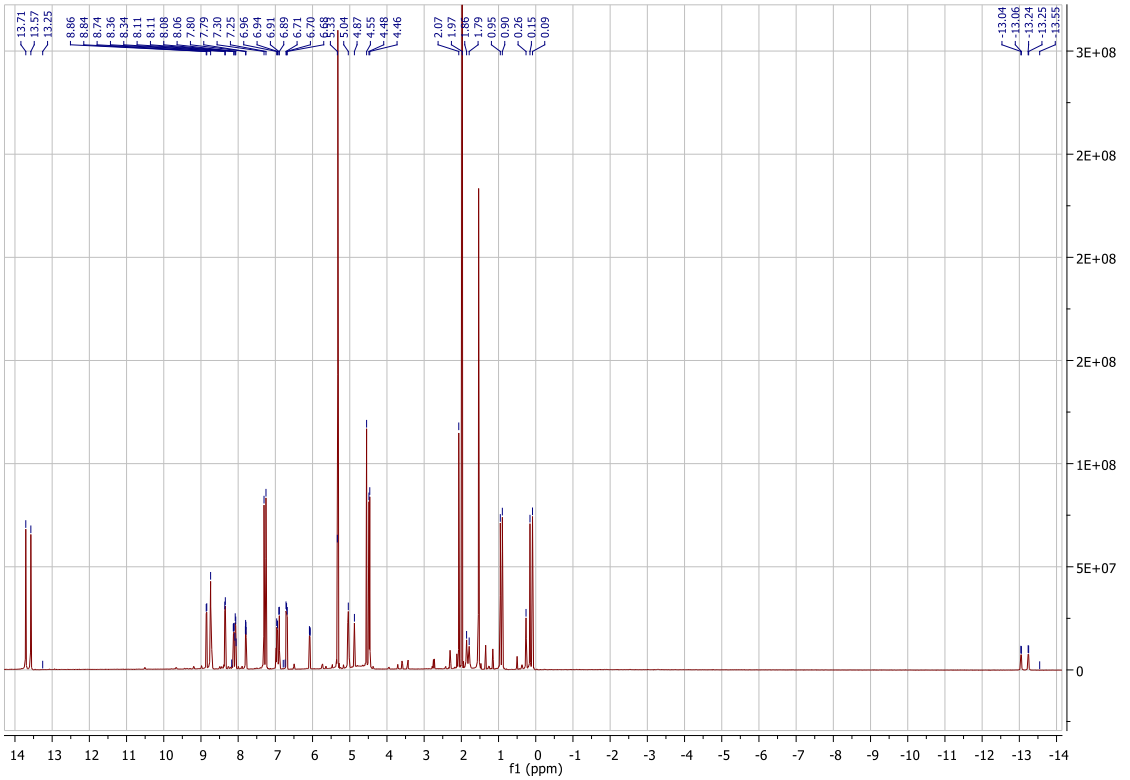

Figures ESI8. ^{1}H NMR spectrum of compound **3** $[Ru_3(\mu_3\text{-}O)(\mu\text{-}OAc)_5\{\mu\text{-}\eta^1(C),\eta^2(N,N)\text{-}dppzCH_3\}(py)_2]PF_6$, recorded from 10^{-2} mol L^{-1} dichloromethane-$_{d2}$ solution.

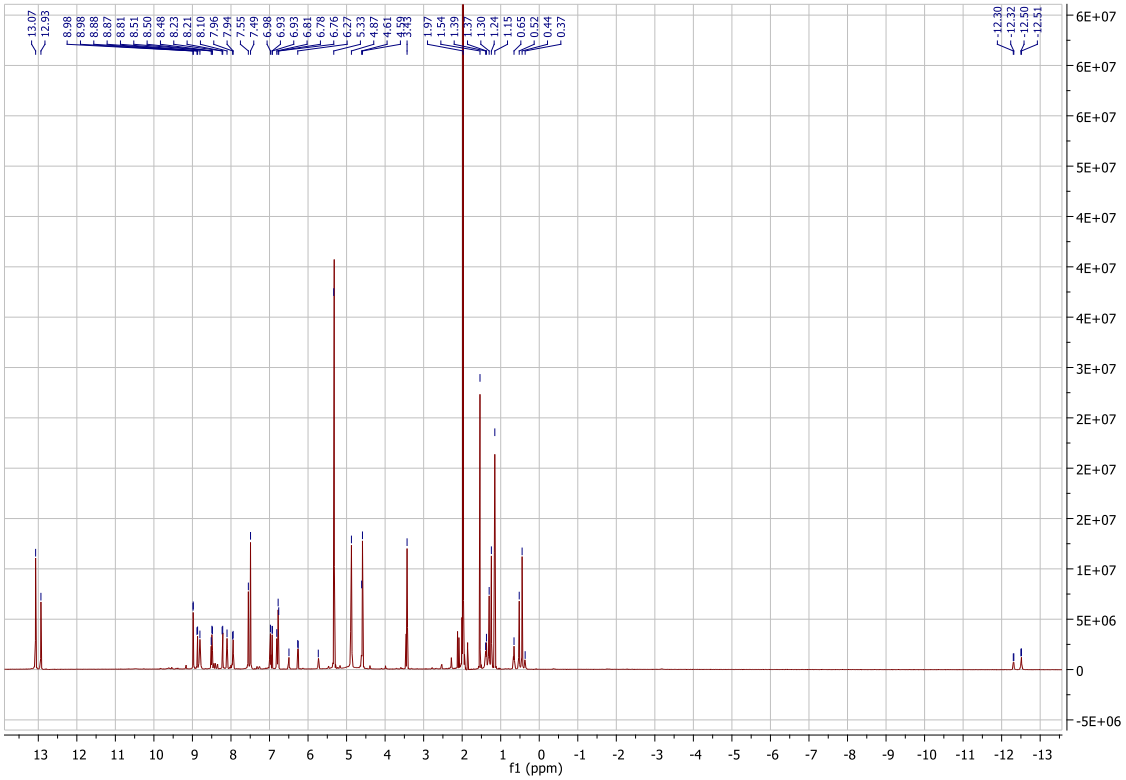

Figures ESI9. ^{1}H NMR spectrum of compound **4** [$Ru_3(\mu_3\text{-}O)(\mu\text{-}OAc)_5\{\mu\text{-}\eta^1(C),\eta^2(N,N)\text{-}dppzCl\}(py)_2]PF_6$, recorded from 10^{-2} mol L^{-1} dichloromethane-$_{d2}$ solution.

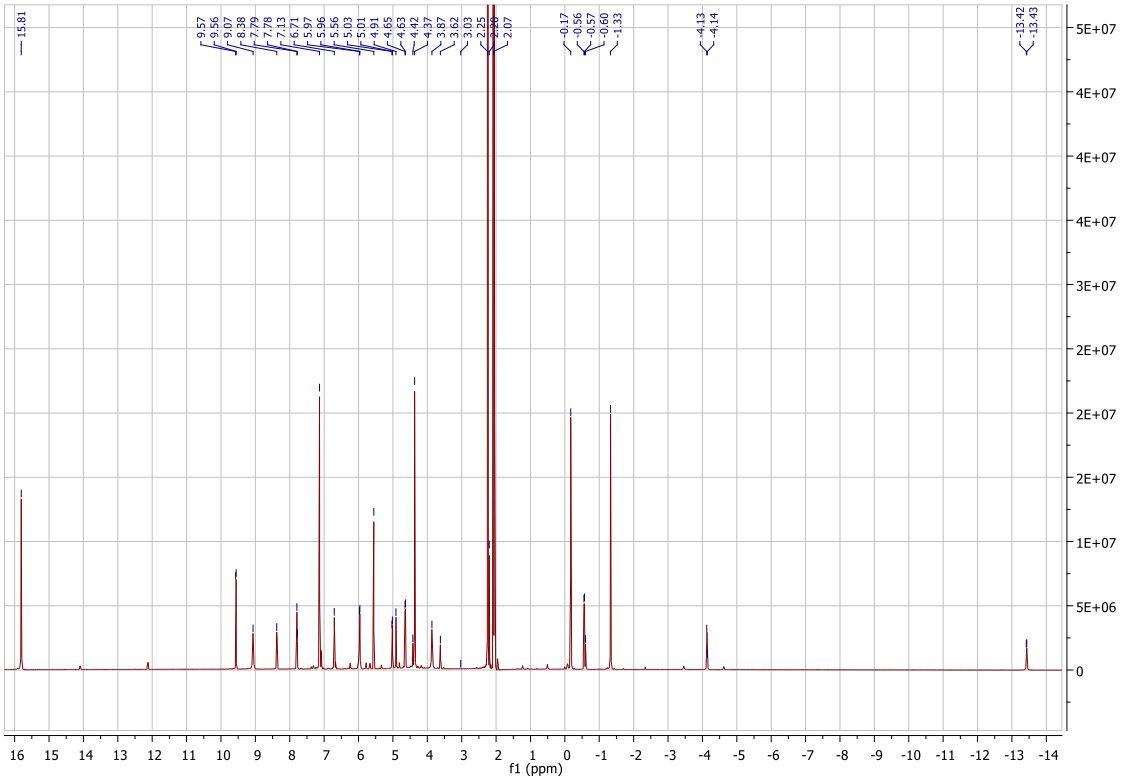

Figures ESI10. ^{1}H NMR spectrum of compound **5** [$Ru_3(\mu_3\text{-}O)(\mu\text{-}OAc)_5\{\mu\text{-}\eta^1(C),\eta^2(N,N)\text{-}phen\}(py)_2]PF_6$, recorded from 10^{-2} mol L^{-1} acetone-$_{d6}$ solution.

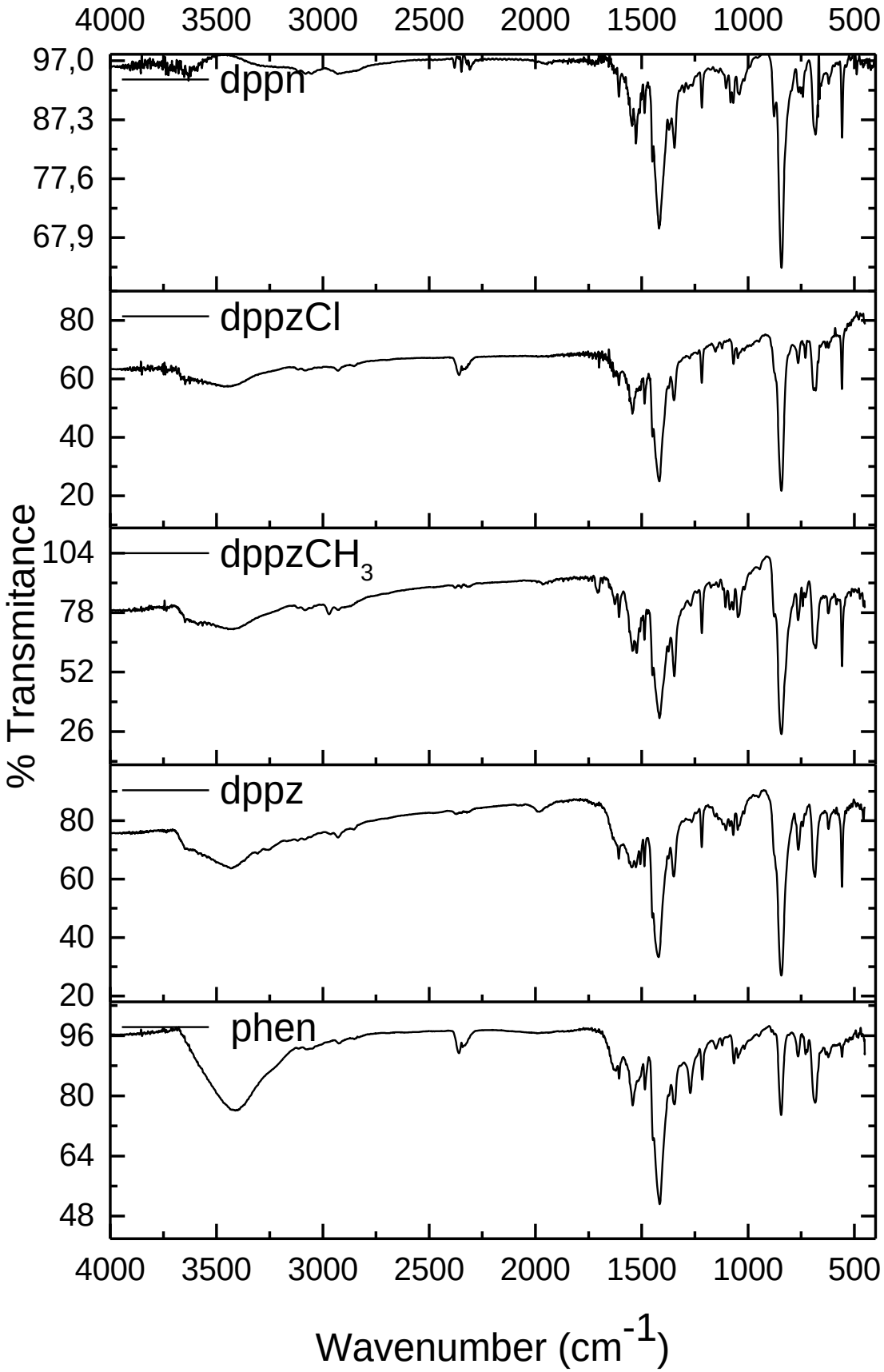

Figure ESI11. Infrared spectra of compounds **1**-**5**, collected in solid state from KBr pellets.

Table ESI 1: Tentative assignment of the main peaks observed in the IR spectra of compounds 1 – 5. All values are presented in cm^{-1} units

1 (dppn)	2 (dppz)	3 (CH_3-dppz)	4 (Cl-dppz)	5 (phen)	
557	555	557	569	569	$\nu_{as}[Ru_3O]$
681	675	680	677	671	δ(OCO)
742	762	769	765	764	ν(CH)
841	843	842	842	844	$\nu_{as}(PF_6)$
____	____	____	925	____	ν(CCl)
1217	1194	1217	1207	1220	ν (CH)
1486	1487	1488	1486	1485	ν(CC)
1345	1351	1352	1352	1344	ν(CN)
1418	1420	1416	1416	1415	$\nu_s(COO^-)$Ac
1543	1546	1544	1543	1541	$\nu_{as}(COO^-)$Ac
1606	1607	1606	1607	1605	$\nu_{as}(COO^-)$Ac
____	3118	3075	3086	3045	ν(CH)

ν – stretching; δ - bending; s= symmetric; as = asymmetric.

Natural Bond Orbitals (NBO) calculations

The NBO stabilization energy is based on concrete Lewis electronic structure from the quantum mechanics treatment (equation 1).

$$\Delta E_{est} = \frac{-q_i \left|F_{ij}\right|^2}{\left(\varepsilon_j^{(NL)} - \varepsilon_i^{(L)}\right)} \quad \text{eq (1)}$$

Where $\varepsilon_j^{(NL)}$ is the energy of the non-Lewis NBO (i.e. π∗); $\varepsilon_j^{(L)}$ is the energy of the orbital occupied by n; q_i is the occupancy of the orbital. The 'stabilization energy' ΔE_{est} is determined by second-order perturbation treatments.[3]

Table ESI 2: Natural Bond Orbital (NBO) information for cluster 2. Stabilization energy values are given in kcal $mol^{-1.}$

Orbitals of spin α	
Donation	**ΣEest (kcal mol-1)**
ruthenium ions – oxo bridge	
n O(55) → n*Ru(56)	76.71
n O(55) → n*Ru(57)	67.41
n O(55) → n*Ru(58)	23.48
n O(55) → BD* O(55)-Ru(58)	42.39
ruthenium – orthometalated	
BD* C(41)-Ru(57) → n*Ru(57)	35.32
ruthenium – acetates	
n O(61) → n*Ru(57)	32.20
n O(60) → n*Ru(57)	74.32
n O(59) → n*Ru(57)	85.09
n O(68) → n*Ru(58)	84.64
n O(65) → n*Ru(58)	90.52
n O(66) → n*Ru(58)	101.93
n O(67) → n*Ru(58)	95.32
n O(63) → n*Ru(56)	44.20
n O(62) → n*Ru(56)	94.21
n O(64) → n*Ru(56)	84.75
ruthenium – pyridine	
n N(39) → n*Ru(56)	64.91
n N(11) → n*Ru(58)	18.71
n N(22) → n*Ru(57)	67.46
Orbitals of spin β	
Donation	**ΣEest (kcal mol-1)**
ruthenium ions – oxo bridge	
n O(55) → n*Ru(56)	86.15
n O(55) → n*Ru(57)	88.38
n O(55) → n*Ru(58)	86.68
ruthenium – orthometalated	
BD* C(41)-Ru(57) → n*Ru(57)	36.49
ruthenium – acetates	
n O(61) → n*Ru(57)	32,61
n O(60) → n*Ru(57)	72,39
n O(59) → n*Ru(57)	81,83
n O(68) → n*Ru(58)	38,82
n O(65) → n*Ru(58)	35.19
n O(66) → n*Ru(58)	30.91
n O(67) → n*Ru(58)	69.44
n O(63) → n*Ru(56)	38.82
n O(62) → n*Ru(56)	72.74
n O(64) → n*Ru(56)	88.42
ruthenium – pyridine	
n N(39) → n*Ru(56)	62.69
n N(11) → n*Ru(58)	64.19
n N(22) → n*Ru(57)	67.14

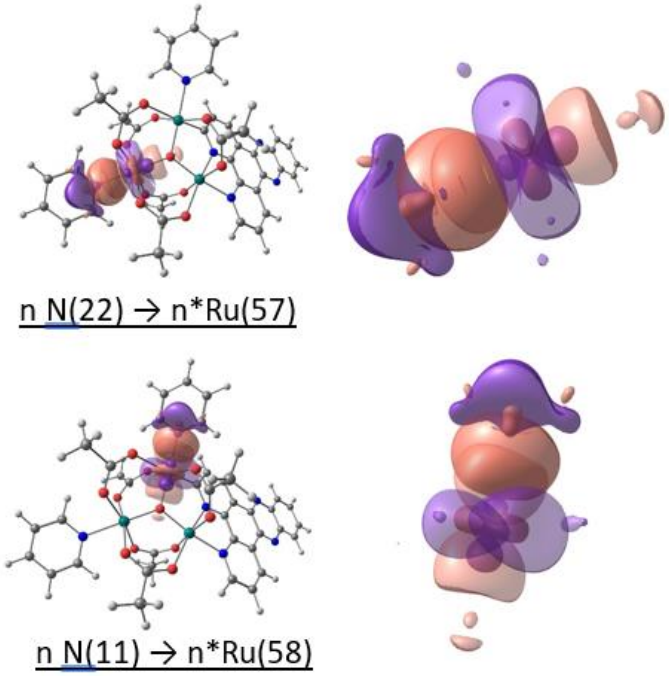

Figure ESI12. Orbitals involved in the pyridine → Ru_3O donation-reception dynamics.

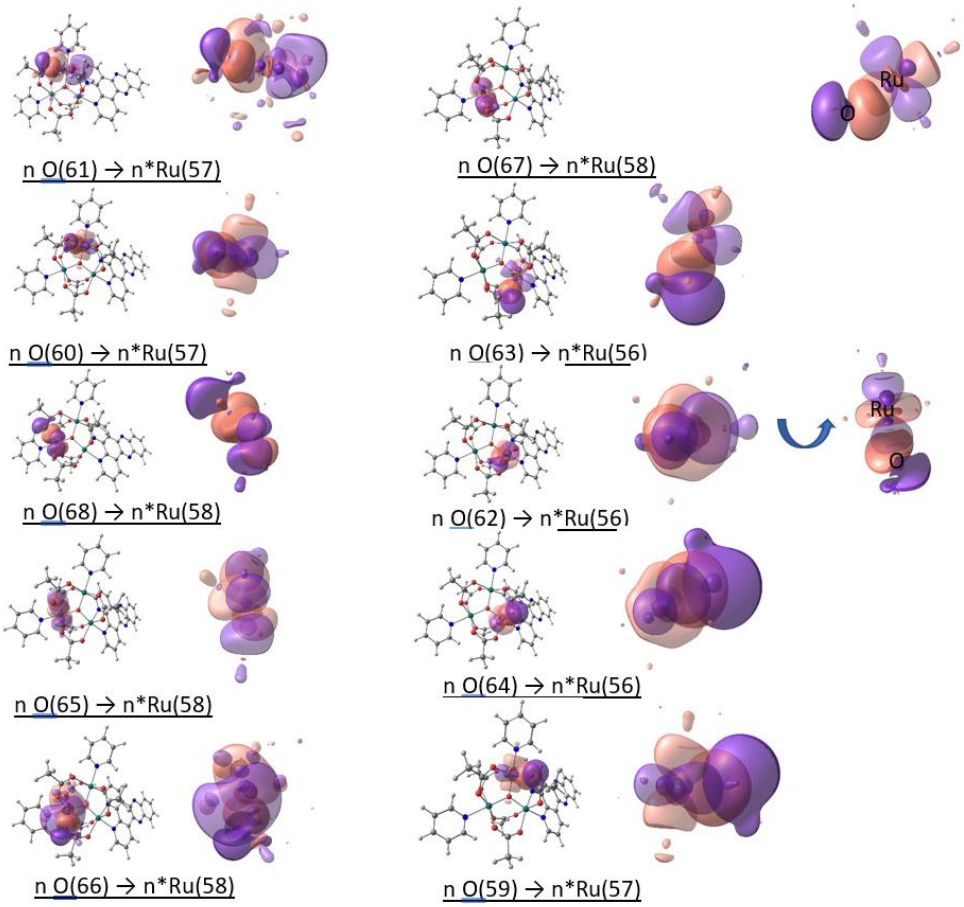

Figure ESI13. Orbitals involved in the acetate → Ru_3O donation-reception dynamics.

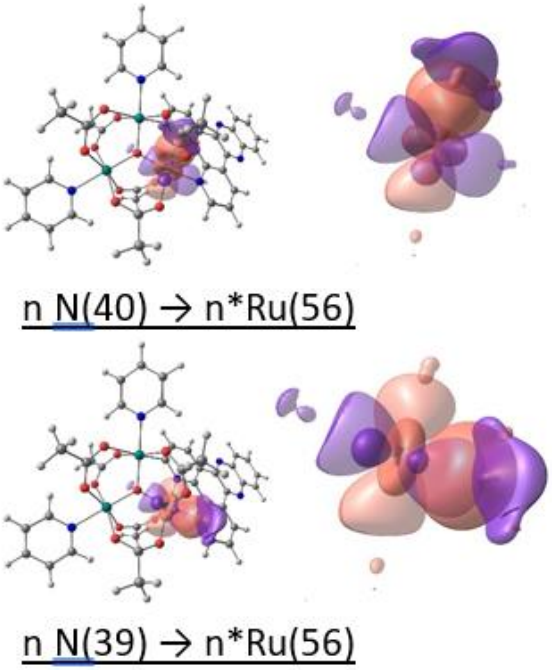

Figure ESI14. Orbitals involved in the dppz → Ru_3O donation-reception dynamics.

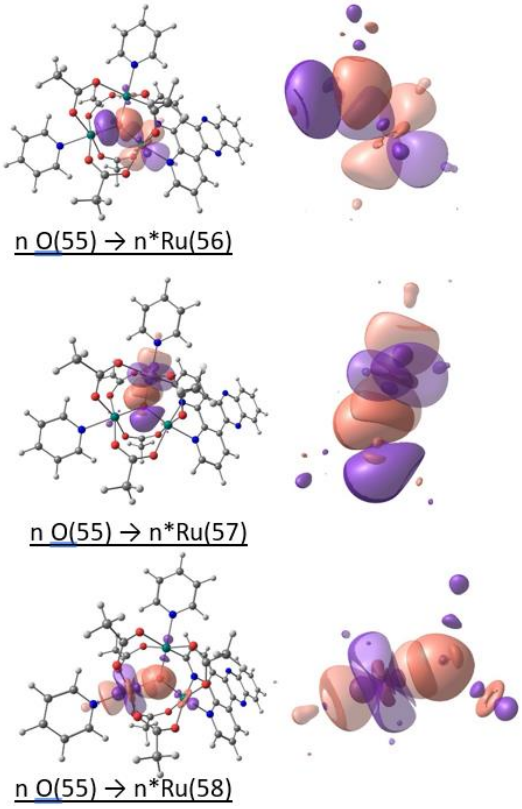

Figure ESI15. Orbitals involved inside the [Ru_3O] donation-reception dynamics.

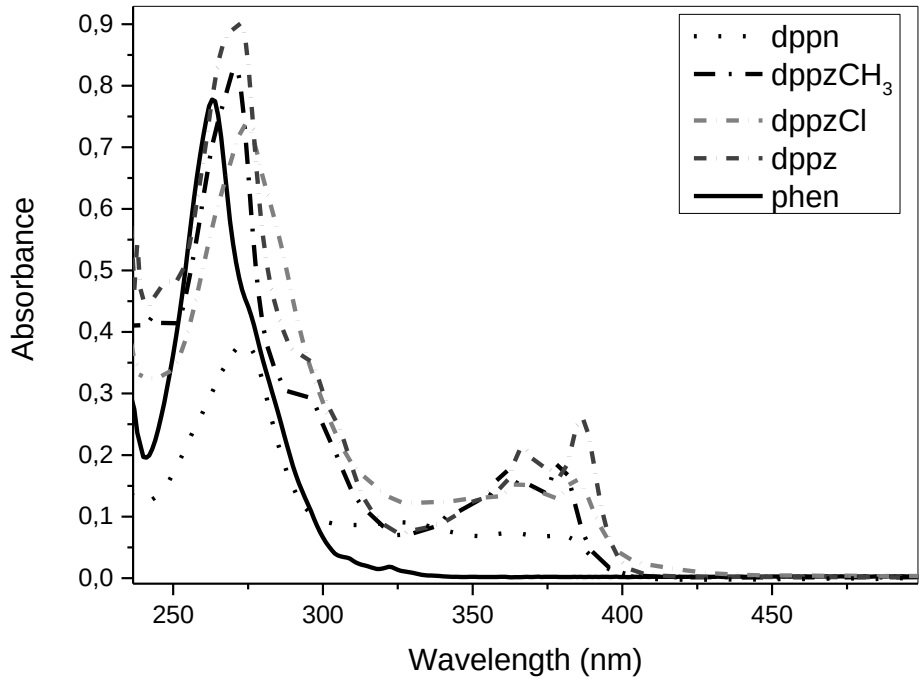

Figure ESI16: Ground-state absorbance spectra of free ligands in DMSO solution.

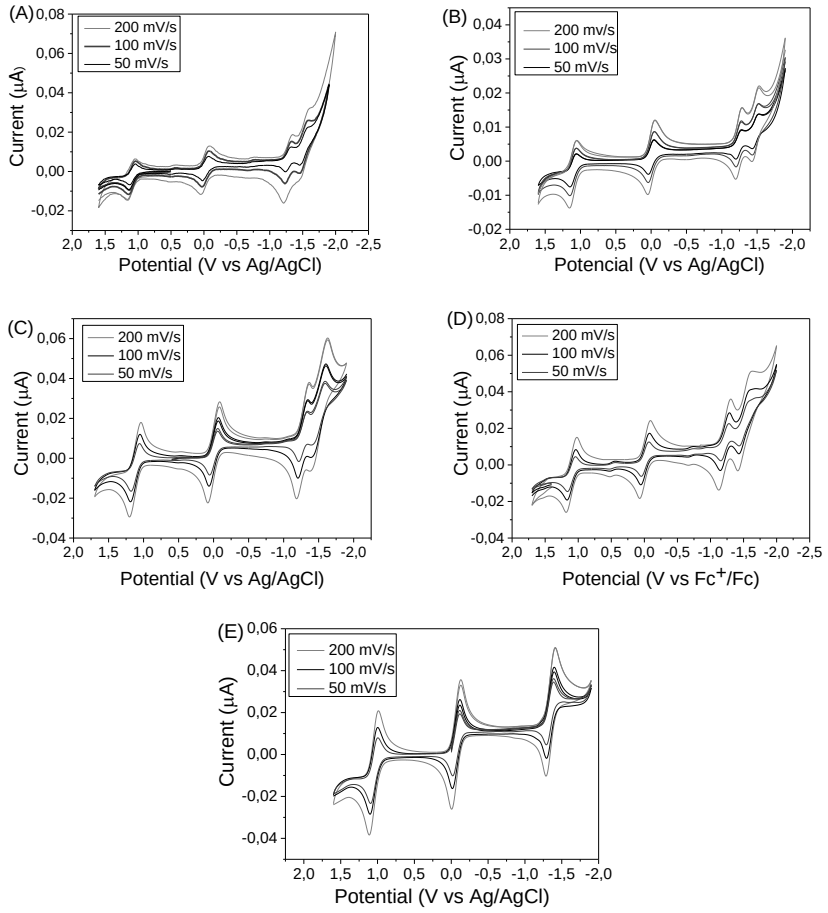

Figure ESI17. Cyclic voltammograms of clusters **1**(A) – **5** (E), in 5,0x10^{-3} M CH_2Cl_2 solutions (0.1 M of NBu_4PF_6).

Determination of ligands pKa (2-4)

The pKa values of ligands (2–4) were determined by experimental procedure using the spectrophotometric method.[1]Buffer solutions were prepared in the pH range from 1.00 to 8.00 by mixing the salts: (Citric Acid Buffer - Na_2HPO_4 and Tris·HCl Buffer, $NH_2C(CH_2OH)_3$.[2] For all solutions, 2% DMSO was used due to the low solubility of the ligands in aqueous medium. Spectral changes were recorded on a spectrophotometer model HP8453, AGILENT, at specific maximum wavelengths of each ligand.

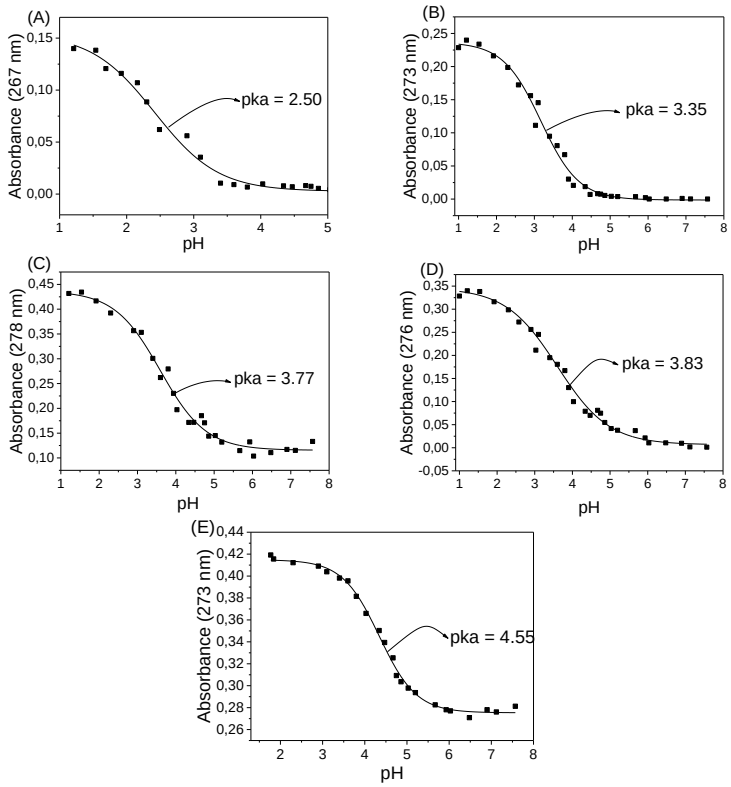

Figure ESI18. Absorbance *vs* pH from spectrophotometric titration of ligands dppn (A), dppz (B), dppzCH_3 (C), dppzCl (D), phen (E).

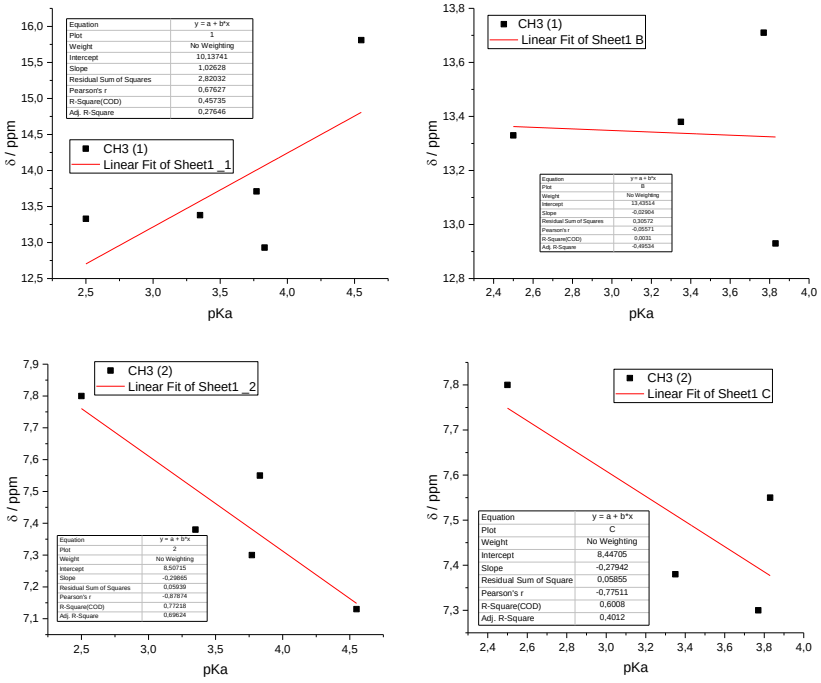

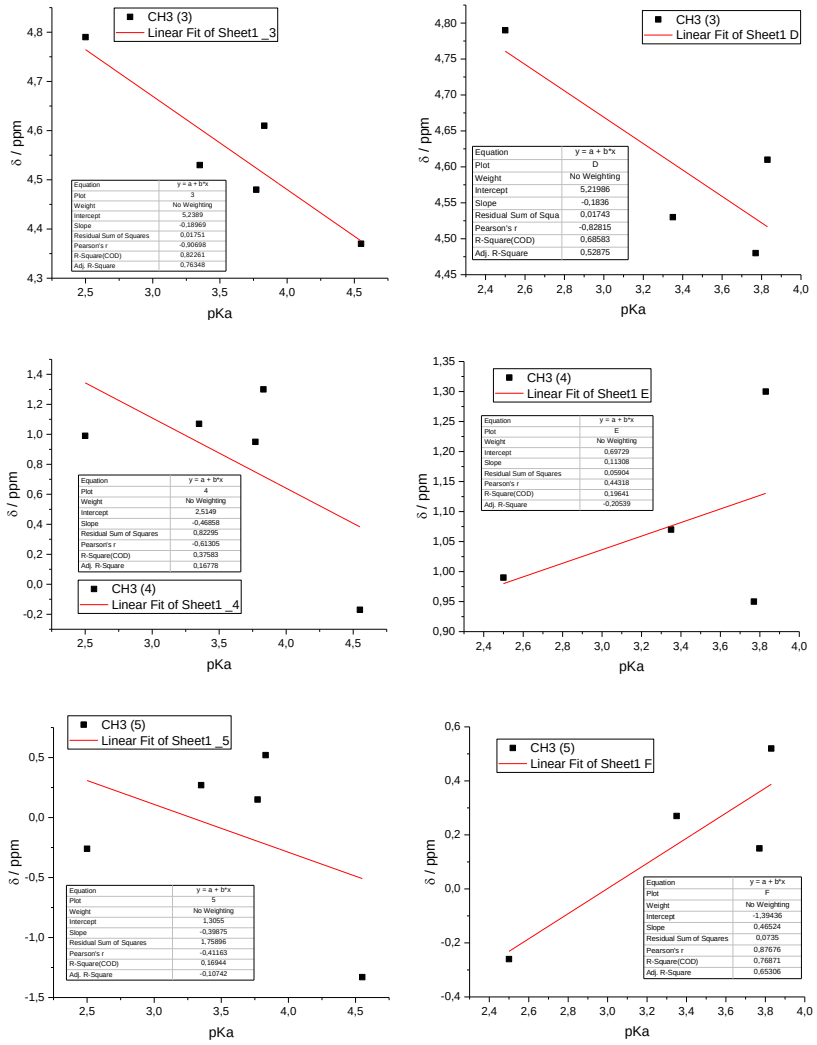

Figure ESI19. Dependence of the methyl hydrogens δ values on the pka of the orthometalated ligands. The first row presents the correlations for the five ligands and the second row presents the correlations without the values of complex **5** (phen ligand).

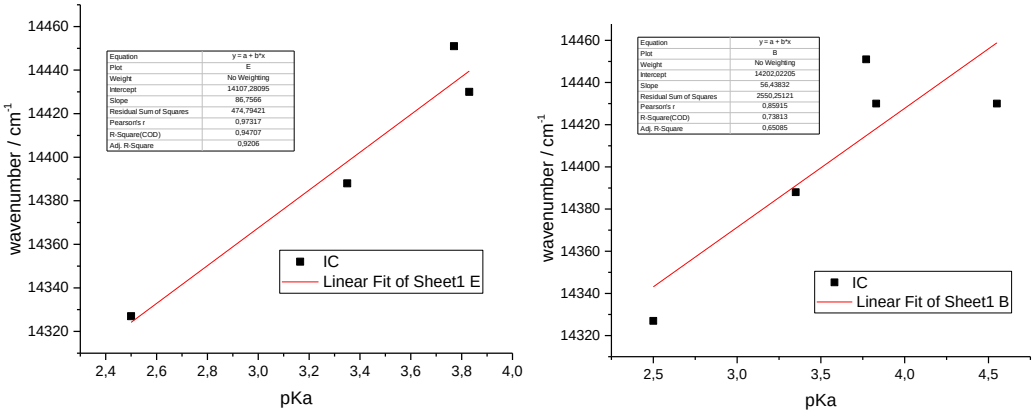

Figure ESI20. Dependence of the IC (Intra-Cluster transition) energy on the pka of the orthometalated ligands. The first plot presents the correlations without the value of complex **5** (phen ligand) and the second plot presents the correlations for the five ligands.

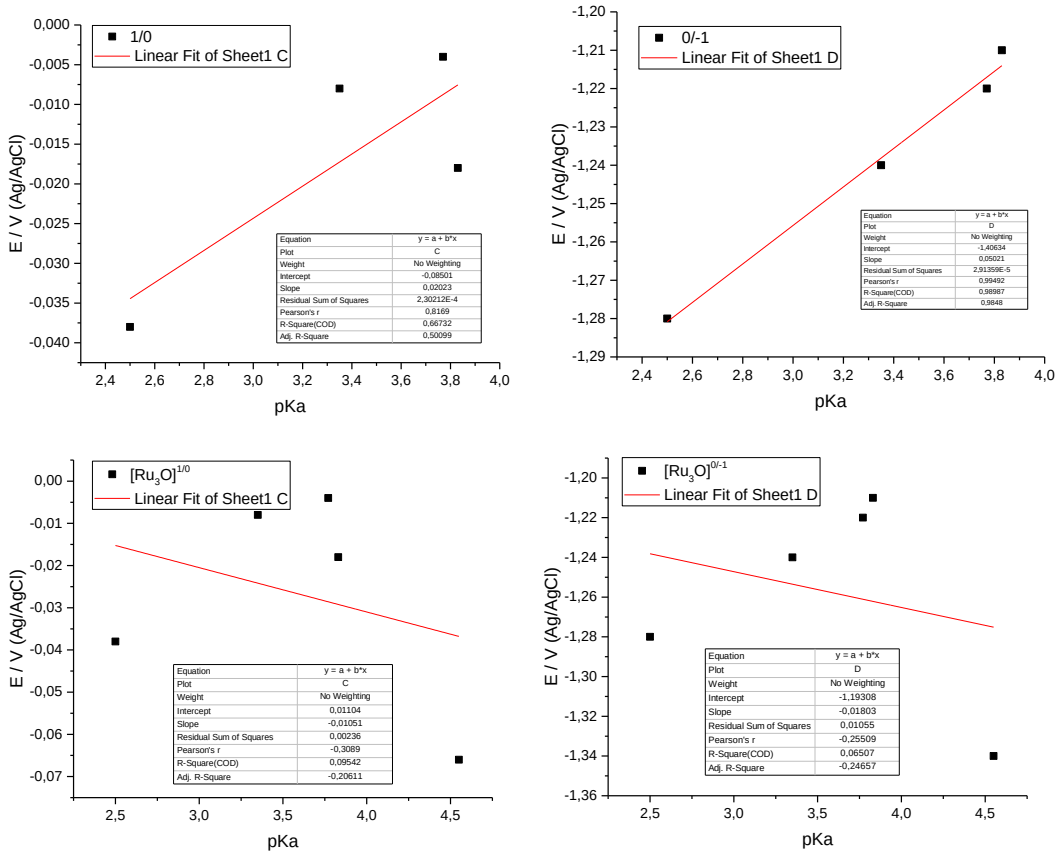

Figure ESI21. Dependence of the $E_{1/2}$values for the monoelectronic redox processes $[Ru_3O]^{1/0/-1}$ on the pka of the orthometalated ligands. The first line presents the correlations without the value of complex **5** (phen ligand) and the second line presents the correlations for the five ligands.

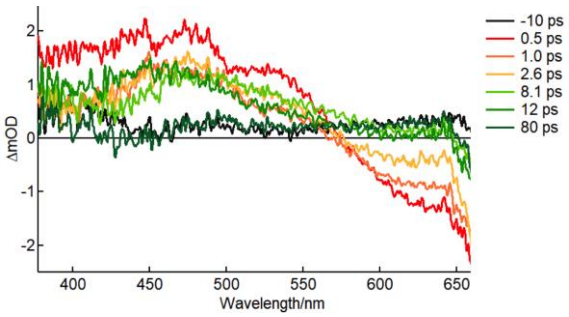

(A)

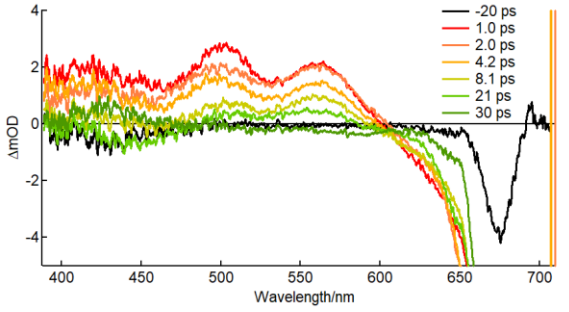

(B)

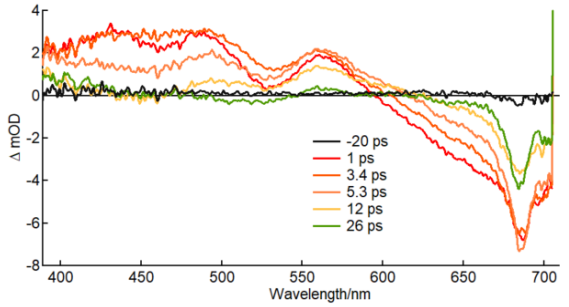

(C)

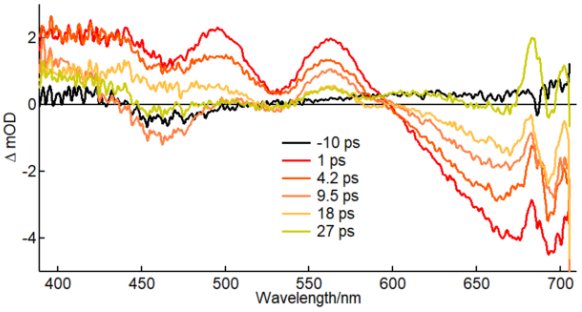

(D)

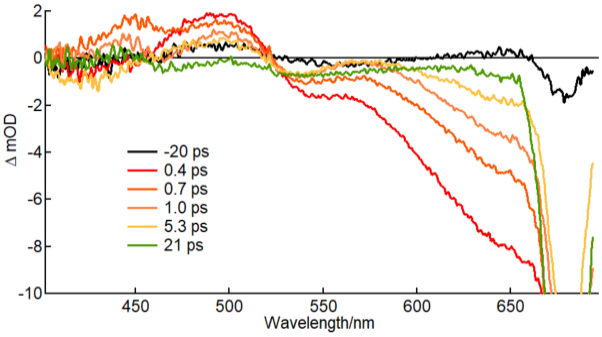

(E)

Figure ESI22.. FsTA spectra of clusters (A) $[Ru_3O(CH_3COO)_6(py)_2MeOH]PF_6$; (B) **2**; (C) **3**; (D) **4** and (E) **5**, in CH_2Cl_2 (λ_{exc} = 700 nm, 4 μJ).

[1] C.J. CUNHA, PhD thesis, University of Sao Paulo, Correlações Espectroscópicas e Eletroquímicas em Clusters Trigonais de Rutênio com Ligantes N-heterocíclicos, 1989.

[2] T. MORITA, M. V. ASSUMPÇÃO, *Manual de soluções, reagentes e solventes; padronização, preparação, purificação*, Edgard Blucher, 1976.

[3] F. Weinhold F. and C. R. Landis, "Discovering Chemistry With Natural Bond Orbitals" John Wiley and Sons Inc. New York, 2012. ISBN: 978-1-118-11996-9.